Key Engineering Materials
ISSN: 1662-9795, Vol. 926, pp 2077-2091
doi:10.4028/p-oeev6l

Submitted: 2021-12-10
Revised: 2022-02-01
Accepted: 2022-02-03
Online: 2022-07-22

Influence of Plastic Deformation on the Hydrogen Embrittlement Susceptibility of Dual Phase Steels

Andreas Drexler[1,a*], Besim Helic[1,b], Zahra Silvayeh[1,c], Christof Sommitsch[1,d], Klemens Mraczek[2,e] and Josef Domitner[1,f]

[1*]Graz University of Technology, Institute of Materials Science, Joining and Forming, Research Group of Lightweight and Forming Technologies, Inffeldgasse 11/I, 8010 Graz, Austria

[2]Voestalpine Stahl GmbH, voestalpine-Straße 3, 4020 Linz, Austria

[a]andreas.drexler@tugraz.at; [b]besim.helic@tugraz.at; [c]zahra.silvayeh@tugraz.at; [d]christof.sommitsch@tugraz.at; [e]klemens.mraczek@voestalpine.com; [f]josef.domitner@tugraz.at

Keywords: Metal forming; Hydrogen; Hydrogen embrittlement; Plastic strain; Dual phase steel;

Abstract. The susceptibility of advanced high-strength steels (AHSS) to hydrogen embrittlement (HE) limits the broad utilization of these materials for body-in-white (BIW) components. The considerable decrease of both ductility and toughness due to local hydrogen accumulation inside of formed components may cause unpredictable time-delayed failure. In particular deep-drawn and punched AHSS components are prone to hydrogen absorption. This work investigates the influence of plastic deformation on hydrogen absorption of dual phase (DP) steels. For that purpose, tensile samples were machined out of three commercial 1.2 mm-thick DP sheets with ultimate tensile strengths of 626 MPa, 826 MPa and 1096 MPa. Samples were uniaxially pre-strained to 2 %, 5 %, 10 %, 15 % and 20 %. After pre-straining the samples were electrochemically charged with hydrogen, and the actual hydrogen contents were determined using a thermal desorption analyser (TDA). Before and after charging, the hardness of the samples was measured and the uniaxial quasi-static tensile properties were determined. In order to quantify the influence of plastic deformation on HE, slow strain rate tests (SSRT) were performed. The results of the tests were correlated with the fraction of martensite determined for each of the three steels.

Introduction

Advanced high-strength steels (AHSS) are characterized by an outstanding combination of high strength, excellent toughness and good formability. AHSS sheets offer promising lightweight potential for the automotive industry, as they allow to reduce the weight and to increase the crash performance of car bodies. However, cold forming and punching of AHSS sheets for body-in-white (BIW) components are compromised by hydrogen embrittlement (HE). Small hydrogen contents can degrade the mechanical properties, especially the ductility. According to Bergmann [1], critical hydrogen uptake may occur along the whole production- and life-cycle of cars, including the processing line of the steel coils, the BIW manufacturing line at the original equipment manufacturer (OEM), or during in-service exposure to the environment. Thus, the lightweight potential of AHSS sheets cannot be fully exploited and certain protective measures must be considered.

Cold forming [2] and punching [3,4] are crucial with respect to HE susceptibility of AHSS sheets, as plastic deformation may increase the solubility [3] and decreases the chemical diffusivity [5,6] of hydrogen. Zones of plastic deformation act like “sponges” and hydrogen accumulates up to five-times more than in bulk zones [3,4,7]. This has different consequences: hydrogen distribution becomes inhomogeneous in the components and, thus, the critical hydrogen content, which is critical for cracking [8], is reached faster. In zones of plastic deformation, the lower chemical diffusion coefficient can aggravate the critical situation, as it causes excess of hydrogen in near-surface regions and it reduces the transport of hydrogen to the bulk. Polyanskiy and co-workers [9,10] described this “hydrogen skin-effect”. According to Nagumo [11], hydrogen-related damage of steels appears as deterioration of the crystal structure rather than void nucleation or microcracking by dislocation motion. He studied the role of plastic straining and dislocation dynamics with and without hydrogen

and proposed a new type of hydrogen embrittlement mechanism, namely the hydrogen-enhanced strain-induced vacancy (HESIV) mechanism. It assumes that hydrogen fosters and stabilizes the formation of excess vacancies in the crystal structure and that the accumulation to vacancy clusters causes brittle macroscopic appearance, although significant plastic straining proceeds fracture on the macroscopic scale.
DP steels are widely used in the automotive industry and fundamentals of the HE susceptibility of AHSS are well studied [12–15]. However, since researchers have mostly been focusing on straining pure ferritic iron, lack of knowledge exists with respect to the influence of plastic deformation on HE of industrial relevant DP steels with high strength and reduced ductility. In comparison to ferritic iron, the composite-like microstructure of DP steels consists of both soft ferrite and hard martensite, which can easily be characterized using scanning electron microscopy (SEM) or light optical microscopy (LOM). Therefore, the present work aims for investigating the role of deformation on the hydrogen solubility of three industrial DP steels. For that purpose, the mechanical properties were characterized before and after hydrogen charging. The charging time until saturation was determined based on pre-recorded absorption curves. The HE susceptibility was measured by slow strain rate testing (SSRT) of hydrogen-charged samples. Comprehensive thermal desorption analysis (TDA) was performed to determine the hydrogen absorption capacity depending on the microstructure, deformation and hydrogen content. Thermal desorption spectroscopy (TDS) and Kissinger's theory supported the categorization of the trapping sites in the microstructures with respect to binding energy and trap density.

Experimental Methods

Materials

Microalloyed DP steels DP600, DP800 and DP1000 with carbon contents < 0.15 wt.%, < 0.18 wt.% and < 0.20 wt.%, respectively, were investigated. Details about the chemical compositions are given elsewhere [16]. The as-delivered sheets with thickness of s = 1.2 mm were galvanized. Microstructure characterization was performed by etching and LOM as published in a previous work [15]. The martensite area fractions f_{M} are summarized in Table 1.

Electrochemical charging

Electrochemical hydrogen charging was performed by immersing samples in H_2SO_4 electrolyte containing 1 g/l Thiourea (TU, CH_4N_2S). Before hydrogen charging, the samples were pickled for 1-2 min in 20 vol% HCl containing 5 g/l Hexamethylenetetramine (HMTA, $C_6H_{12}N_4$) to remove zinc coatings and oxide layers from the surfaces. HMTA was added to the solution to prevent corrosion of the samples and to avoid hydrogen uptake during pickling [16]. A cylindrical platinum counter electrode was used for electrochemical charging. The mesh electrode had a diameter of 40 mm and height of 50 mm. The current density i = 0.1 A/dm² (1 mA/cm²) was constant. Hydrogen charging was performed for 2 hours in order to reach homogeneous hydrogen distribution within the samples. After charging, the samples were rinsed with ethanol and dried with compressed air. The laboratory temperature of 22 ± 3 °C and the electrolyte temperature were monitored during each charging sequence.

Quasi-static tensile and hardness testing

Quasi-static uniaxial tensile tests according to standard DIN EN ISO 6892-1 were conducted using a Zwick/Roell Z100 uniaxial testing machine for characterizing the basic mechanical properties of the as-delivered DP steels. Smooth samples were machined according to DIN 50125 – H (gauge length l_0 = 80 mm, gauge width w = 20 mm and sample thickness s = 1.2 mm). The tensile directions of the samples were 0° (RD), 45° (DD) and 90° (TD) to the rolling direction. Before and after hydrogen charging, Vickers hardness HV5 was determined at the surface of the samples using an Emco-Test DuraScan G5 hardness tester. The Vickers hardness of each sample was determined by averaging the hardness values of 120 indentations. Before charging, samples used for hardness measurements were ground and polished, which reduced the thickness of the samples to s = 1.1 mm. Charging the as-

polished samples was performed as described in section “Electrochemical charging”. The handling time of the samples between end of charging and start of the hardness measurements was less than 5 min.

Slow strain rate testing

Slow strain rate testing (SSRT) was performed to characterize the ductility and the strength after hydrogen charging. The tests were performed using a Zwick/Roell Z100 uniaxial tensile machine with the crosshead speed of 0.5 mm/min (~10^{-4} s^{-1}). Smooth tensile samples were machined according to DIN 50125 – H with the gauge length of l_0 = 50 mm, the gauge width of w = 12.5 mm and sample thickness s = 1.2 mm. The sample axis was parallel to RD. Hydrogen charging was performed individually for each sample, as described in section “Electrochemical charging”. The handling time of the samples between end of charging and start of SSRT was less than 2 min. SSRT was performed under atmospheric conditions and without additional zinc coating of the samples. For evaluating the influence of the strength and the microstructure on the HE susceptibility of the industrial DP steels, the HE index, $HE\%$, was calculated as

$$HE\% = 1 - \frac{A_{l,H}}{A_l}, \tag{1}$$

where A_{50} and $A_{50,H}$ are the fracture strains measured without charging and after hydrogen charging, respectively. With increasing HE susceptibility $HE\%$ increases towards unity.

Thermal desorption analysis and spectroscopy

For measuring the hydrogen content c_H, thermal desorption analysis (TDA) was performed using a Brucker G8 Galileo analyser. The machine is equipped with a thermal conductivity sensor (TCS) and an infrared furnace (IF). The helium gas-calibrated TCS has an accuracy of around 0.1 wppm/g sample. Before charging, the weight of each sample was measured using a high-precision scale. The charging procedure is described in the previous section “Electrochemical charging”. The handling time of the samples between end of charging and start of TDA was less than 2 min. The hydrogen content was measured by heating the charged samples in the IF from room temperature (RT) to 600 °C linearly with a constant heating rate of 1 K/s. The hydrogen content $c_{H,BM}$ of the as-delivered base material (BM) was determined using rectangular samples with length of 100 mm in RD, width of 15 mm in TD and thickness of 1.2 mm. The rectangular samples were wire-cut.

Figure 1: DP1000 samples at different strains.

For studying the influence of plastic deformation on the hydrogen content $c_{H,PS}$, tensile samples as used for SSRT were pre-strained as illustrated Figure 1. The increase of the absorption capacity due to pre-straining was evaluated by calculating the difference in the hydrogen content Δc_H as

$$\Delta c_H = c_{H,PS} - c_{H,BM}. \tag{2}$$

In addition, microstructural trapping sites were characterized by thermal desorption spectroscopy (TDS). TDS spectra were recorded from RT to 900 °C using different heating rates θ, namely 0.3 K/s (18 K/min), 0.6 K/s (36 K/min) and 1.0 K/s (60 K/min). For measuring the sample temperature accurately thermocouple of type K was placed next to the sheet samples in the IF. The gas flow between the sample position in the IF to the TCS lasted 16 s and was considered in the evaluation. As demonstrated by Drexler et al. [17], the evaluation procedure according to Kissinger's theory can be applied for single or well separated TDS peaks. The activation energy E_D of the chemical diffusion coefficient [17] was determined by

$$E_D = R \frac{d(\ln(\theta/T_{max}^2))}{d(1/T_{max})}, \tag{3}$$

where R is the universal gas constant and T_{max} is the temperature at the peak maxima, which was determined in a straight forward manner as function of the applied heating rates θ. The activation energy according to Kissinger' theory was often misinterpreted as the thermal energy, which is necessary for hydrogen desorption from trapping sites. Due to the more generalized thermodynamic concept of Kissinger's theory [18], E_D is the activation energy for bulk hydrogen diffusion, if hydrogen diffuses from the interior of the sample to the surface [19,20].

Result and Discussion

Characterization of basic mechanical properties

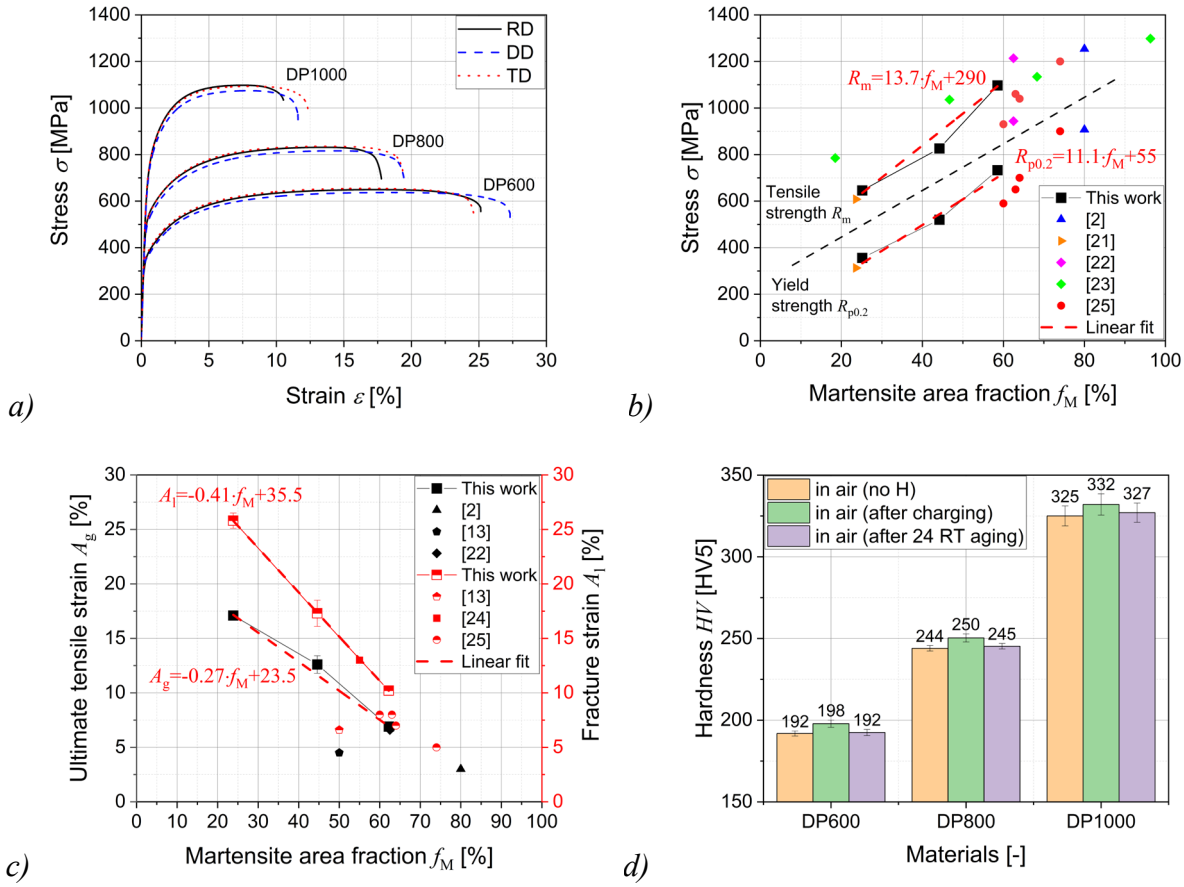

Figure 2: a) Engineering stress-strain curves measured in different directions. b) Yield strength and ultimate tensile strength as function of martensite area fraction [2,12,21–23]. *c) Ultimate tensile strain and fracture strain as function of martensite area fraction* [2,13,21,22,24,25]. *d) Measured Vickers hardness before and after charging.*

Figure 2a shows the engineering stress-strain curve measured in each of the three directions RD, DD and TD. The ultimate tensile strength was comparatively low in DD, while the ultimate tensile strengths in RD and TD were higher and almost equal. The martensite area fractions f_{M} and the corresponding measured mechanical properties in RD are summarized in Table 1. The martensite area fractions were 25 ± 5 % for DP600, 44 ± 5 % for DP800 and 59 ± 5 % for DP1000. Figure 2b shows the linear increase of both the yield strength and the ultimate tensile strength with increasing f_{M}. Linear fitting of the measured yield strength $R_{\mathrm{p0.2}}$ and of the ultimate tensile strength R_{m} gives

$$R_{\mathrm{p0.2}} = 11.1\, f_{\mathrm{M}} + 55 \tag{4}$$

$$R_{\mathrm{m}} = 13.7\, f_{\mathrm{M}} + 290. \tag{5}$$

The R^2-values, which quantify the quality of the fits, are 0.962 for Eq. (4) and 0.999 for Eq. (5). Literature data added to Figure 2b are in good agreement with the measured trend of the tensile properties. Differences in strength of around 200 MPa between literature sources arise from different alloying concepts and processing routes of the steels. The $R_{\mathrm{m}}/R_{\mathrm{p0.2}}$ ratios decrease just slightly from 1.8 for DP600 to 1.6 for DP800 to 1.5 for DP1000 and are independent of the investigated directions. The ratio corresponds with the strain hardening coefficient n. With increasing strain hardening the resistance against plastic deformation increases and causes a more homogeneous distribution of plastic deformation within components. The macroscopic effect of localized plastic deformation and its role on the inhomogeneous hydrogen distribution in notched samples was recently demonstrated for AHSS in the work of Drexler et al. [26].

Figure 2c presents the measured ultimate tensile strains A_{g} and fracture strains A_{l}, which decrease with increasing martensite area fraction f_{M}. Linear fitting of A_{g} and A_{l} gives

$$A_{\mathrm{g}} = -0.27\, f_{\mathrm{M}} + 23.5 \tag{6}$$

$$A_{\mathrm{l}} = -0.41\, f_{\mathrm{M}} + 35.5. \tag{7}$$

The R^2-values of the fitted linear curves are 0.978 and 0.999 for Eq. (6) and Eq. (7), respectively. A_{g} is always smaller than A_{l} and the differences are 8.7 % for DP600, 4.7 % for DP800 and 3.3 % for DP1000. The difference in strain is a measure for necking in the tensile test before fracture. With only small or without any necking brittle fracture would occur. Literature data added to Figure 2c are less consistent with the measured trend of the strains.

Although, the correlation of the mechanical properties of DP steels with the martensite area/volume fraction is well known [15], such steels contain also significant amounts of microalloying elements. The steels used in the present study were alloyed with titanium and niobium to nucleate carbides in the matrix during tempering [27–29]. Those carbides contribute to the total strength due to precipitation strengthening [30,31]. They are also known as beneficial for the HE resistance of AHSS [19,20,32–34].

Table 1: Mechanical properties in RD, martensite area fraction and hydrogen uptake of the as-delivered DP steels.

Properties	DP600	DP800	DP1000	Reference
Martensite area fraction f_M [%]	25 ± 5	44 ± 5	59 ± 5	[15]
Hydrogen content $c_{H,BM}$ [wppm]	2.07 ± 0.31	2.20 ± 0.12	2.67 ± 0.19	[15]
Yield strength $R_{p0.2}$ [MPa]	356 ± 3	520 ± 2	733 ± 3	This work
Ultimate tensile strength R_m [MPa]	646 ± 3	826 ± 5	1097 ± 1.5	This work
Ratio of ultimate tensile strength and yield strength $R_m/R_{p,0.2}$ [-]	1.8	1.6	1.5	This work
Ultimate tensile strain A_g [%]	17.1 ± 0.3	12.6 ± 0.8	6.9 ± 0.2	This work
Fracture strain A_l [%]	25.8 ± 0.7	17.3 ± 1.2	10.2 ± 0.4	This work

For a comprehensive investigation of the influence of hydrogen on the mechanical properties of DP steels, Vickers hardness (HV5) measurements were conducted on as-polished surfaces before and after charging. As shown in Figure 2d, the average Vickers hardness before hydrogen charging was 192 HV5 for DP600, 244 HV5 for DP800 and 325 HV5 for DP1000. Hydrogen charging caused an increase of the Vickers hardness by about 6 HV5. Although this effect is small, the hardness increase seems to be independent of the microstructure. A similar observation was done by Depover et al. [35] applying nanoindentation and hydrogen plasma charging. To ensure that the increase in hardness attributes to hydrogen in the microstructure and not to the formation of oxide layers, further hardness measurements were performed after aging for 24 hours at room temperature (RT). During this time hydrogen desorbed from the surfaces of the samples, as measured by Drexler et al. [15]. 24 hours after charging the hardness decreased again to the initial values of the as-polished samples. Hence, the increase in hardness was reversible and it can be attributed to the hydrogen content of the microstructure.

The role of hydrogen on the strength of ferritic and martensitic steels is a long-lasting discussion and for a comprehensive overview the authors reference to the book of Nagumo [11]. Macroscopic hardening, as observed in the present work, could be explained by a strong interaction of interstitial hydrogen atoms with dislocations. Most likely the strain fields around hydrogen atoms and around dislocations attract each other [36,37], which cause the formation of Cottrell clouds being dragged by moving dislocations and increase the critical resolved shear stress.

Classification of hydrogen embrittlement susceptibility

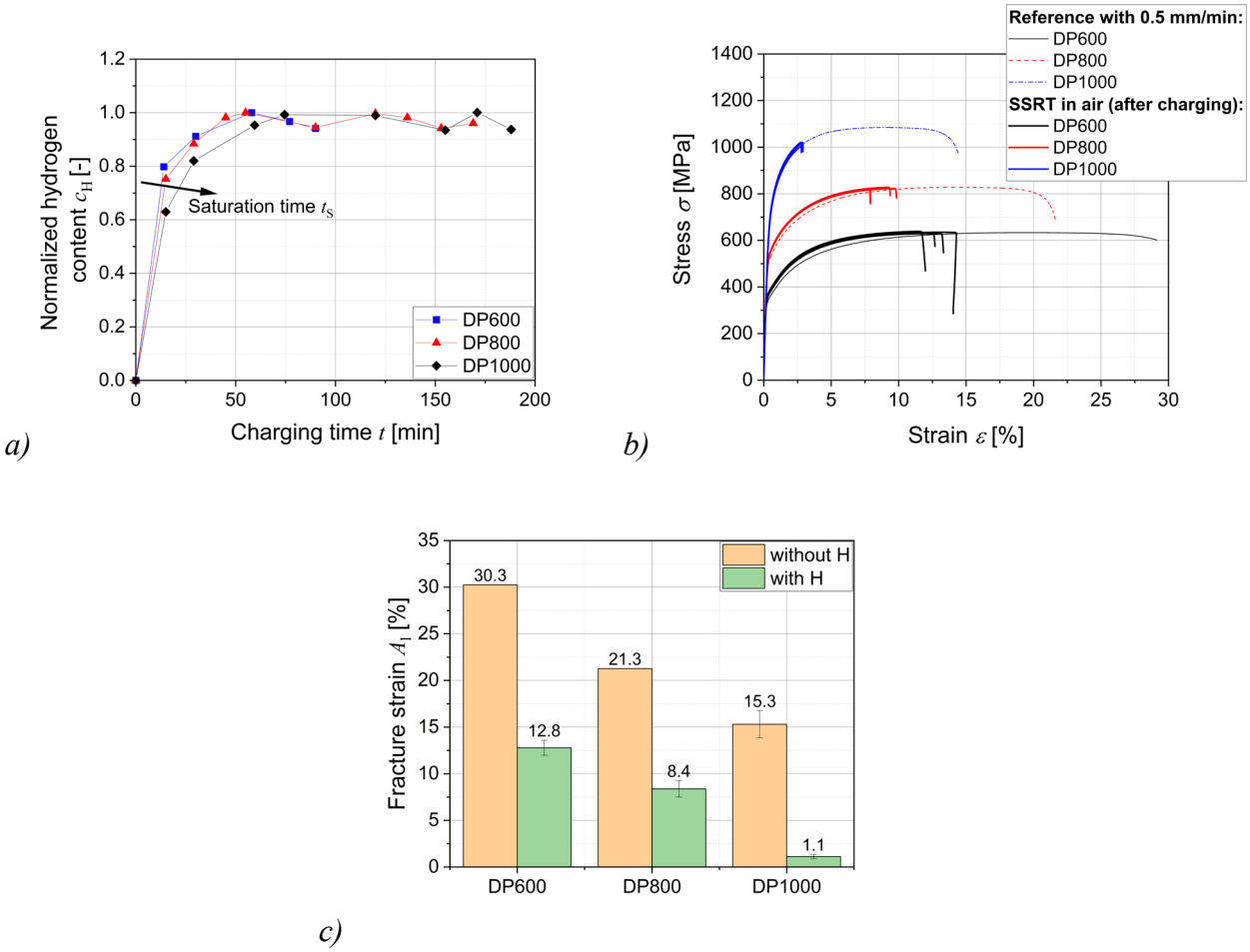

Figure 3: a) Hydrogen content as function of charging time. b) Hydrogen degradation of engineering stress-strain curves in RD measured by SSRT. c) Fracture strain of the as-delivered DP steels before and after charging.

For evaluating the role of the material strength on the HE susceptibility, smooth tensile samples were charged with hydrogen. In contrast to notched sample geometries, smooth samples have homogenous stress distribution, since they do not face the problem of hydrogen accumulation by maxima in the hydrostatic stress fields and by localized plastic deformation at the notch [2,3,26]. For guaranteeing also homogeneous hydrogen distribution after charging, the minimum time to reach saturation was determined as shown in Figure 3a. For better comparison of the charging time dependency, the absorption curves were normalized with the stationary hydrogen contents of 2.07 wppm for DP600, 2.20 wppm for DP800 and 2.67 wppm for DP1000, as given in Table 1. Due to the high bulk diffusivity and the low sheet thickness of 1.2 mm, the hydrogen content increased rapidly during charging and the stationary value was reached after the charging time of around 75 min. Thus, a conservative hydrogen charging time of 120 min was applied for all subsequent samples. As shown in Figure 3a, DP600 reached its hydrogen saturation faster than DP800 and DP1000. The kinetics of hydrogen uptake depend on the hydrogen absorption rate at the surface and on the hydrogen trapping capacity of the microstructure. In general, hydrogen trapping causes an increase of the hydrogen solubility and a decrease of the bulk diffusivity [5,6]. The bulk diffusivity has to be distinguished from the tracer diffusivity of hydrogen in ferritic iron [5,38]. For DP steels it is in the range between 10^{-5} mm²/s and 10^{-2} mm²/s depending on the hydrogen content [12,22,39,40]. Figure 3b shows the recorded stress-strain curves of the SSRT. While the bold lines were determined without hydrogen charging, the thin lines represent the SSRT after hydrogen charging. The SSRT were repeated three-times for each material and the reproducibility was good. Due to the high hydrogen contents of more than 2 wppm (Table 1), the fracture strain was significantly reduced for each of the three DP steels,

while the ultimate tensile strength was less affected. As indicated by the measured increase in hardness, also an increase in strength can be seen in Figure 3b. Nevertheless, further measurements are necessary for improving the statistical certainty and for quantifying the change in yield strength and strain hardening by hydrogen.

In the present work the HE susceptibility of DP steels was characterized based on the fracture strain, since the fracture strain is reported in literature as the most HE-sensitive quantity [21,22,25]. As summarized in Figure 3c, due to HE the fracture strain decreased from 30.3 % to 12.8 % for DP600, from 21.3 % to 8.4 % for DP800 and from 15.3 % to 1.1 % for DP1000. However, the fracture strain seems to be less microstructural sensitive (as shown in Figure 2c) and depends on the sample geometry and strain rate. This makes a direct comparison with literature data difficult. The applied crosshead displacement speed of 0.5 mm/min, which corresponds to an average strain rate of 10^{-4} s^{-1}, was relatively high compared to measurements on DP steels reported in literature [21,23]. Only Koyama et al. [24] used even higher strain rates of 10^{-3} s^{-1} for evaluating the HE susceptibility. The strain rate dependency of the HE susceptibility is well known. The characterization of a true threshold as function of the hydrogen content would require either the use of smaller strain rate (e.g., about 10^{-7} s^{-1}) or the application of constant load tests (CLT) [2] instead of SSRT. Drexler et al. [26] proved that the strain rate limit for bulk diffusion-controlled SSRT is theoretically about 10^{-7} s^{-1}. Lower strain rates cause a macroscopically stationary hydrogen distribution throughout the SSRT. However, desorption during SSRT with small strain rates affects the hydrogen distribution in the samples. Moreover, these tests are generally time-consuming and thus expensive. Zinc coatings, which are applied after charging, can prevent hydrogen losses during testing, but also cause a decrease of the hydrogen content by desorption during sample handling between charging and galvanization. Furthermore, reliable theories to model the effect of zinc coatings on the hydrogen distribution within the samples and on the measured hydrogen susceptibility are still missing in literature to the authors knowledge [15]. Anyway, the effect of HE was very pronounced in the present investigations using higher strain rates for SSRT, which is partially related to minimum hydrogen losses during sample handling and testing. Therefore, the evaluation of the HE index, as demonstrated in Figure 4a, can be regarded as a qualitative measure for the susceptibility, but cannot be interpreted as a true threshold. According to Eq. (1) the HE index increases with increasing f_M and thus with increasing R_m. Although the correlation between A_l and f_M was linear as shown in Figure 2c, the increase of the HE index was non-linear. In other words, the susceptibility was more pronounced at higher strength, as shown in Figure 4b.

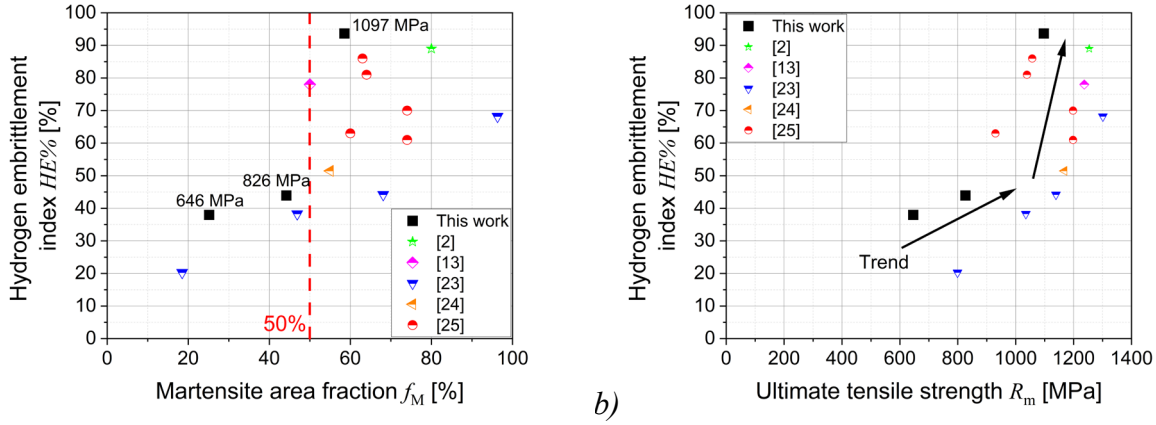

Figure 4: Hydrogen embrittlement indices of dual phase steels as function of a) martensite area fraction and b) ultimate tensile strength [2,13,23,24,41].

Most scholars evaluated the HE susceptibility of DP steels by using Eq. (1). Only Liu et al. [41] referenced the HE index to the reduction in fracture area R_A instead of the fracture strain A_l. Anyway, a comparison is valid, because Depover et al. [21] demonstrated that both fracture strain and fracture area give similar experimental trends. Literature data were added to Figure 4a and 4b. Obviously, HE of DP steels can occur independently of the ultimate tensile strength, but materials with R_m > 1000

MPa seem to be much more susceptible, as the HE indices are larger than 50% and as they increase more with further increase of R_m.
The HE indices were high for the investigated hydrogen contents of around 2 wppm, but a correlation with the martensite area fraction in the microstructure could not be clearly found. For better interpretation, the applied methods for evaluating the HE susceptibility need to be better understood and improved to be more sensitive to microstructural changes rather than sensitive to changing testing parameters. The interaction of plasticity and hydrogen content during SSRT is one of the main issues, which is further investigated in the following sections. The large scatter of the measured HE indices could be related to differences in charging and testing parameters as well as in the microstructural resistance to HE. Furthermore, different charging procedures were applied. For example, Wang et al. [23] and Liu et al. [41] equipped their tensile testing machines with electrochemical cells to perform in-situ charging rather than charging before SSRT. Since SSRT combined with in-situ charging requires additional time for hydrogen uptake and bulk diffusion, they applied lower strain rates of 10^{-6} s^{-1} and of 10^{-8} s^{-1}, respectively.

Measurement of Hydrogen Absorption Capacity

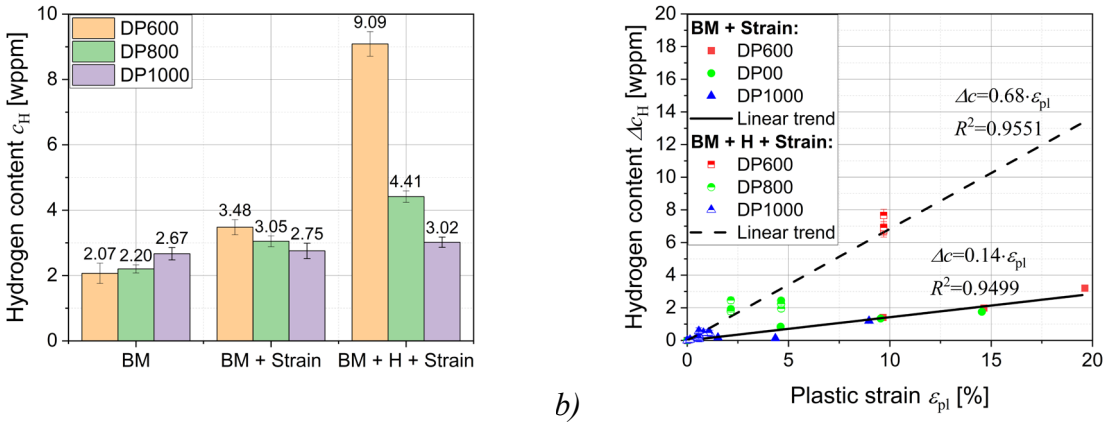

a) *b)*

Figure 5: a) Hydrogen content of the non-strained base material (BM), and after straining without hydrogen (BM+Strain) and after straining with hydrogen: (BM+H+Strain). DP600 was strained to 10%, DP800 was strained to 5% and DP1000 was strained to 1%. b) Increase in hydrogen absorption capacity as function of plastic strain..

As shown in Figure 5a, the hydrogen content $c_{H,BM}$ of the base material (BM) increases almost linearly with R_m. Drexler et al. [15] assumed that hard martensite grains absorb almost three-times more hydrogen than soft ferrite grains and that the rule of mixture applies. Straining of the BM before charging (BM + Strain) increased the hydrogen content. DP600 with largest A_l was strained to 10 %, while DP800 and DP1000 with lower A_l were strained to 5 % and to 1 %, respectively. The hydrogen content $c_{H,PS}$ was correlated with the plastic strain. $c_{H,PS}$ increased from 2.07 to 3.48 wppm for DP600, from 2.20 to 3.05 wppm for DP800, and from 2.67 to 2.75 wppm for DP1000.
Straining of charged samples (BM + H + Strain) had an even more pronounced effect: $c_{H,PS}$ increased from 2.07 to 9.09 wppm for DP600, from 2.20 to 4.41 wppm for DP800, and from 2.67 to 3.02 wppm for DP1000. Between straining and hydrogen charging, the samples were aged at RT for 24 hours. Therefore, hydrogen was able to desorb from the surface before an additional charging sequence was applied. TDA measurements performed after aging at RT for 24 hours revealed a remaining hydrogen content of < 0.1 wppm. Thus, the additional charging sequence was not the reason for the excessive hydrogen absorption.
As shown in Figure 5b, the hydrogen absorption capacity Δc_H depends linearly on the plastic strain ε_{pl}. The slopes of the fitted lines increase from 0.14 to 0.63 wppm/% when hydrogen is present during straining. This increase in the hydrogen absorption capacity associated with plastic straining cannot be explained simply by dislocation multiplication. Strain induces most likely additional point defects,

when hydrogen is present. The results confirm the interaction of hydrogen content and plastic straining for industrial DP steels. Straining of AHSS with R_m > 1000 MPa makes investigations difficult. It is shown that studying DP steels with different R_m allows extrapolation to higher plastic strains. The interaction of hydrogen content and plastic straining has several consequences with respect to the HE susceptibility:

- The increase of the hydrogen content indicates an increase of the defect density in the microstructure that traps hydrogen.
- The difference between in-situ and ex-situ charging to evaluate the HE susceptibility is more complex and cannot be described only by the difference in bulk diffusion. Furthermore, steady hydrogen absorption at the surface while samples are plastically strained most likely cause inhomogeneous distribution of point defects and thus hydrogen distribution inside the samples.
- Forming or punching of sheet metals should always be performed under minimum hydrogen contents. Plastic straining in the presence of hydrogen causes an irreversible increase in the hydrogen solubility and may reduce the resistivity of the final component to HE.

Identification of Hydrogen Trapping Sites

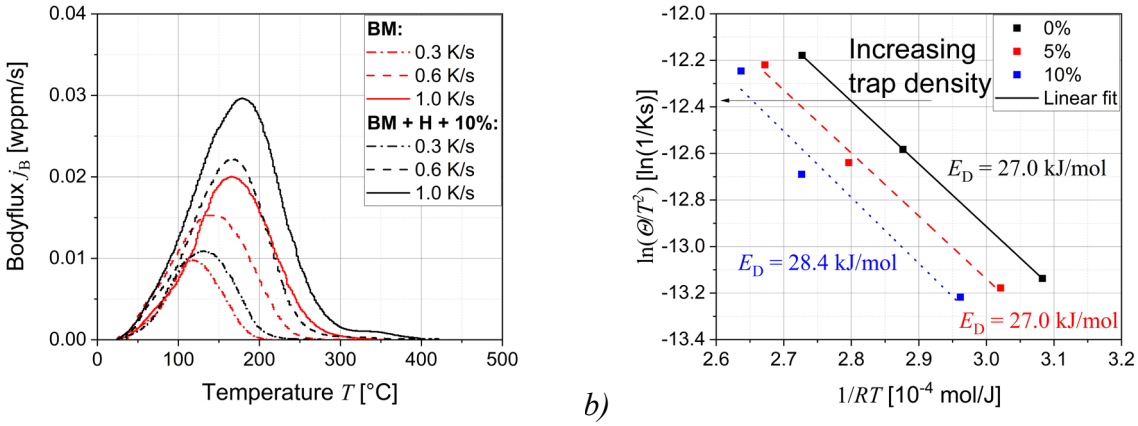

a) *b)*

Figure 6: a) Thermal desorption spectroscopy (TDS) of DP1000 as function of heating rate and plastic strain. b) Choo-Lee plot to determine the hydrogen desorption energy and the evolution of trap densities.

The samples were uniaxially strained in RD, which caused a linear increase of the hydrogen content with plastic strain (see Figure 5b). Plastic straining introduces additional dislocations most likely in soft ferrite grains, which can trap large amounts of hydrogen. Hard martensite grains contain normally high dislocation densities close to the theoretical limit of 10^{15} m/m³. Figure 6a shows the change of recorded TDS spectra of DP1000 when samples were strained to 10 % before charging. The TDS peak maxima shift with straining to higher temperatures and also the areas under the curves increase. The latter correlates with the hydrogen content and the applied heating rates ranging from 0.3 to 1.0 K/s. An evaluation of the TDS peak maxima according to Kissinger's theory is shown Figure 6b, which is also known as Choo-Lee plot. The evaluated activation energy of $E_D \approx 28$ kJ/mol is virtually independent of the plastic strain. This value is very similar to the activation energies frequently quoted by Choo and Lee [42], who were first measuring the effect of dislocations on the activation energy for hydrogen bulk diffusion in pure iron. Drexler et al. [5,6] confirmed their results by evaluating permeation curves of cold formed iron samples. The increase in trap density due to plastic straining is assumed to shift the linear curves in the Choo-Lee plot to lower RT^{-1}-values. In other words, the energy gain of hydrogen by trapping at defects depends on the type and not on the density of the defects.

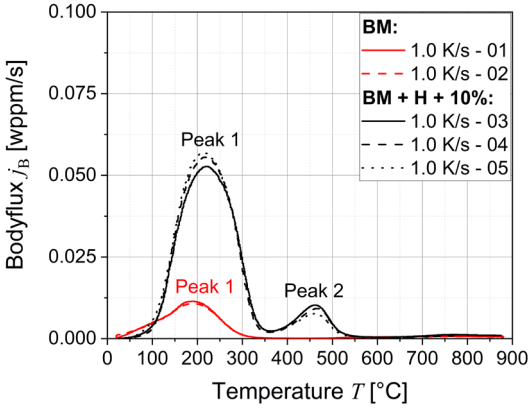

Figure 7: TDS spectra of DP600 as function of strain.

The interaction of hydrogen with dislocations is crucial to fully understand the HE mechanisms also on macroscopic scale. The effect of straining of hydrogen-charged samples was even more pronounced for hydrogen absorption, which cannot be explained only by dislocation multiplication. In addition, point defect formation during dislocation motion must be considered. Figure 7 shows preliminary TDS spectra of strained and hydrogen-charged (BM + H) samples compared to TDS spectra recorded for unstrained (BM) samples. Two clearly separated peaks occur in the (BM + H) TDS spectrum, which were confirmed by three independent measurements. While straining of uncharged samples to 10 % increased the first TDS peak as outlined by the multiplication of dislocations, straining of hydrogen-charged samples lead to a second TDS peak at 450 °C. The first peak moderately increased and was shifted to higher temperatures. The second peak indicates that additional point defects such as vacancies [43,44] may nucleate in the microstructure during straining if hydrogen is present. Further measurements will be conducted to investigate the nature of the second peak and to correlate the results of SSRT with recorded TDS spectra.

Summary

The present work investigates the role of hydrogen and plastic deformation on the hydrogen embrittlement (HE) susceptibility. For that purpose, three industrial DP steels with thickness of 1.2 mm and ultimate tensile strengths of 626 MPa, 826 MPa and 1096 MPa were investigated by tensile testing, Vickers hardness measurements and slow strain rate tests (SSRT). Comprehensive TDA and TDS measurements were performed and the results were correlated with the HE susceptibility. The following conclusions can be drawn according to the results of these experiments:

- Classification of the HE susceptibility of DP steels revealed a strong correlation with the ultimate tensile strength. However, the correlation with the martensite area fraction is less pronounced.
- Hydrogen causes a reversible increase in hardness, which is explained by a strong interaction of hydrogen with dislocations increasing the critical resolved shear strength.
- Plastic strain increases the hydrogen absorption capacity of DP steels. The increase is influenced by the DP microstructure, the plastic strain level and the hydrogen content being present during straining.
- The activation energy according to Kissinger's theory was 28 kJ/mol and stays unaffected by the level of plastic strain.
- An additional high temperature peak was measured in the recorded TDS spectra. Most likely this peak is caused by the strong interaction between hydrogen and moving dislocations intensifying the dislocation multiplication during plastic straining and enhances the strain-induces nucleation of further point defects.

In future investigations will be conducted to reveal the nature of the second TDS peak and to derive new damage models for evaluating the HE risks of cold formed DP steel components.

Nomenclature

A_g	Ultimate tensile strain [%]
A_l	Fracture strain for gauge length l [%]
$A_{l,H}$	Fracture strain after hydrogen charging [%]
AHSS	Advanced high-strength steels
BIW	Body-in-white
BM	Base material
c_H	Hydrogen content [wppm]
$c_{H,BM}$	Hydrogen content of the base material [wppm]
$c_{H,PS}$	Hydrogen content of plastically deformed material [wppm]
Δc_H	Increase in hydrogen content by plastic strain [wppm]
DD	Diagonal direction
DP	Dual phase
θ	Heating rate [°C/s]
E_D	Activation energy according to Kissinger's theory [kJ/mol]
ε	Strain [%]
ε_{pl}	Plastic strain [%]
f_M	Martensite area fraction [%]
HE	Hydrogen embrittlement
$HE\%$	Hydrogen embrittlement index [-]
HMTA	Hexamethylenetetramine
HV	Vickers hardness [HV5]
j_B	Bodyflux [wppm/s]
l	Length [mm]
l_0	Gauge length [mm]
LOM	Light optical microscopy
OEM	Original equipment manufacturer
R	Universal gas constant [kJ/Kmol]
RD	Rolling direction
$R_{p0.2}$	Yield strength [MPa]
R_m	Ultimate tensile strength [MPa]
s	Sheet thickness [mm]
SSRT	Slow strain rate test
σ	Stress [MPa]
T	Temperature [°C]
T_{max}	Temperature of the TDS peak maximum [°C]
TD	Transverse direction
TDA	Thermal desorption analysis
TDS	Thermal desorption spectroscopy
TU	Thiourea
w	Width [mm]

References

[1] C. Bergmann, Hydrogen embrittlement resistance of advanced high strength steel grades in automotive applications, Ruhr-Universität Bochum, 2020.

[2] A. Drexler, C. Bergmann, G. Manke, V. Kokotin, K. Mraczek, M. Pohl, W. Ecker, On the local evaluation of the hydrogen susceptibility of cold-formed and heat treated advanced high strength steel (AHSS) sheets, Mater. Sci. Eng. A. 800 (2021) 140276. https://doi.org/10.1016/j.msea.2020.140276.

[3] A. Drexler, C. Bergmann, G. Manke, V. Kokotin, K. Mraczek, S. Leitner, M. Pohl, W. Ecker, Local hydrogen accumulation after cold forming and heat treatment in punched advanced high strength steel sheets, J. Alloys Compd. 856 (2021) 158226. https://doi.org/10.1016/j.jallcom.2020.158226.

[4] A. Drexler, W. Ecker, N. Winzer, K. Mraczek, V. Kokotin, G. Manke, C. Bergmann, A step towards numerical evaluation of the local hydrogen susceptibility of punched and cold-formed advanced high strength steel (AHSS) sheets, in: L. Duprez (Ed.), SteelyHydrogen, Ocas, 2018: p. A02. http://steelyhydrogen2018proc.be/articles/pdf/2.

[5] A. Drexler, W. Siegl, W. Ecker, M. Tkadletz, G. Klösch, H. Schnideritsch, G. Mori, J. Svoboda, F.D. Fischer, Cycled hydrogen permeation through Armco iron – A joint experimental and modeling approach, Corros. Sci. 176 (2020) 109017. https://doi.org/10.1016/j.corsci.2020.109017.

[6] W. Siegl, W. Ecker, J. Klarner, G. Kloesch, G. Mori, A. Drexler, G. Winter, H. Schnideritsch, Hydrogen trapping in heat treated and deformed Armco iron, in: NACE - Int. Corros. Conf. Ser., 2019: pp. 1–12.

[7] B. Ozdirik, T. Suter, U. Hans, T. Depover, K. Verbeken, P. Schmutz, L.P.H. Jeurgens, H. Terryn, I. De Graeve, Study of the hydrogen uptake in deformed steel using the microcapillary cell technique, Corros. Sci. 155 (2019) 55–66. https://doi.org/10.1016/j.corsci.2019.04.029.

[8] A. Drexler, S. He, R. Pippan, L. Romaner, V.I. Razumovskiy, W. Ecker, Hydrogen segregation near a crack tip in nickel, Scr. Mater. 194 (2021) 113697. https://doi.org/10.1016/j.scriptamat.2020.113697.

[9] V.A. Polyanskiy, A.K. Belyaev, E.L. Alekseeva, A.M. Polyanskiy, D.A. Tretyakov, Y.A. Yakovlev, Phenomenon of skin effect in metals due to hydrogen absorption, Contin. Mech. Thermodyn. 31 (2019) 1961–1975. https://doi.org/10.1007/s00161-019-00839-2.

[10] V.A. Polyanskiy, A.K. Belyaev, A.A. Chevrychkina, E.A. Varshavchik, Y. u. A. Yakovlev, Impact of skin effect of hydrogen charging on the Choo-Lee plot for cylindrical samples, Int. J. Hydrogen Energy. 46 (2021) 6979–6991. https://doi.org/10.1016/j.ijhydene.2020.11.192.

[11] M. Nagumo, Fundamentals of Hydrogen Embrittlement, Springer Singapore, Singapore, 2016. https://doi.org/10.1007/978-981-10-0161-1.

[12] Q. Liu, J. Venezuela, M. Zhang, Q. Zhou, A. Atrens, Hydrogen trapping in some advanced high strength steels, Corros. Sci. 111 (2016) 770–785. https://doi.org/10.1016/j.corsci.2016.05.046.

[13] J. Rehrl, K. Mraczek, A. Pichler, E. Werner, Mechanical properties and fracture behavior of hydrogen charged AHSS/UHSS grades at high- and low strain rate tests, Mater. Sci. Eng. A. 590 (2014) 360–367. https://doi.org/10.1016/j.msea.2013.10.044.

[14] R.G. Davies, Influence of martensite content on the hydrogen embrittlement of dual-phase steels, Scr. Metall. 17 (1983) 889–892. https://doi.org/10.1016/0036-9748(83)90255-7.

[15] A. Drexler, B. Helic, Z. Silvayeh, K. Mraczek, C. Sommitsch, J. Domitner, The role of hydrogen diffusion, trapping and desorption in dual phase steels, J. Mater. Sci. (2022) 1–30. https://doi.org/10.1007/s10853-021-06830-0.

[16] J. Hu, Y. Wang, L. Yu, Y. Zou, Y. Wang, An Investigation of a Combined Thiourea and Hexamethylenetetramine as Inhibitors for Corrosion of N80 in 15% HCl Solution: Electrochemical Experiments and Quantum Chemical Calculation, Int. J. Corros. 2015 (2015). https://doi.org/10.1155/2015/548031.

[17] A. Drexler, L. Vandewalle, T. Depover, K. Verbeken, J. Domitner, Critical verification of the Kissinger theory to evaluate thermal desorption spectra, Int. J. Hydrogen Energy. 46 (2021) 39590–39606. https://doi.org/10.1016/j.ijhydene.2021.09.171.

[18] R. Kirchheim, Bulk Diffusion-Controlled Thermal Desorption Spectroscopy with Examples for Hydrogen in Iron, Metall. Mater. Trans. A Phys. Metall. Mater. Sci. 47 (2016) 672–696. https://doi.org/10.1007/s11661-015-3236-2.

[19] A. Drexler, T. Depover, K. Verbeken, W. Ecker, Model-based interpretation of thermal desorption spectra of Fe-C-Ti alloys, J. Alloys Compd. 789 (2019) 647–657. https://doi.org/10.1016/j.jallcom.2019.03.102.

[20] A. Drexler, T. Depover, S. Leitner, K. Verbeken, W. Ecker, Microstructural based hydrogen diffusion and trapping models applied to Fe–C X alloys, J. Alloys Compd. 826 (2020) 154057. https://doi.org/10.1016/j.jallcom.2020.154057.

[21] T. Depover, D. Pérez Escobar, E. Wallaert, Z. Zermout, K. Verbeken, Effect of hydrogen charging on the mechanical properties of advanced high strength steels, Int. J. Hydrogen Energy. 39 (2014) 4647–4656. https://doi.org/10.1016/j.ijhydene.2013.12.190.

[22] T. Schaffner, A. Hartmaier, V. Kokotin, M. Pohl, Analysis of hydrogen diffusion and trapping in ultra-high strength steel grades, J. Alloys Compd. 746 (2018) 557–566. https://doi.org/10.1016/j.jallcom.2018.02.264.

[23] Z. Wang, J. Liu, F. Huang, Y. Bi, S. Zhang, Hydrogen Diffusion and Its Effect on Hydrogen Embrittlement in DP Steels With Different Martensite Content, Front. Mater. 7 (2020) 359–364. https://doi.org/10.3389/fmats.2020.620000.

[24] M. Koyama, C.C. Tasan, E. Akiyama, K. Tsuzaki, D. Raabe, Hydrogen-assisted decohesion and localized plasticity in dual-phase steel, Acta Mater. 70 (2014) 174–187. https://doi.org/10.1016/j.actamat.2014.01.048.

[25] Q. Liu, Q. Zhou, J. Venezuela, M. Zhang, A. Atrens, Hydrogen Concentration in Dual-Phase (DP) and Quenched and Partitioned (Q&P) Advanced High-Strength Steels (AHSS) under Simulated Service Conditions Compared with Cathodic Charging Conditions, Adv. Eng. Mater. 18 (2016) 1588–1599. https://doi.org/10.1002/adem.201600217.

[26] A. Drexler, J. Domitner, C. Sommitsch, Modeling of Hydrogen Diffusion in Slow Strain Rate (SSR) Testing of Notched Samples, in: P. V.A., B. A.K. (Eds.), Adv. Hydrog. Embrittlement Study, 143rd ed., Springer, 2021: pp. 87–111. https://doi.org/10.1007/978-3-030-66948-5_6.

[27] T. Depover, K. Verbeken, Evaluation of the effect of V4C3 precipitates on the hydrogen induced mechanical degradation in Fe-C-V alloys, Mater. Sci. Eng. A. 675 (2016) 299–313. https://doi.org/10.1016/j.msea.2016.08.053.

[28] A. Drexler, B. Oberwinkler, S. Primig, C. Turk, E. Povoden-Karadeniz, A. Heinemann, W. Ecker, M. Stockinger, Experimental and numerical investigations of the γ″ and γ′ precipitation kinetics in Alloy 718, Mater. Sci. Eng. A. 723 (2018) 314–323. https://doi.org/10.1016/j.msea.2018.03.013.

[29] A. Drexler, H.P. Gänser, W. Ecker, B. Oberwinkler, A. Fischersworring-Bunk, Computationally efficient models for the forced air cooling of turbine disks, in: Therm. Process Model. - Proc. from 5th Int. Conf. Therm. Process Model. Comput. Simulation, ICTPMCS 2014, 2014: pp. 223–231.

[30] A. Drexler, A. Fischersworring-Bunk, B. Oberwinkler, W. Ecker, H.-P. Gänser, A microstructural based creep model applied to alloy 718, Int. J. Plast. 105 (2018) 62–73. https://doi.org/10.1016/j.ijplas.2017.11.003.

[31] A. Drexler, W. Ecker, R. Hessert, B. Oberwinkler, H.-P. Gänser, J. Keckes, M. Hofmann, A. Fischersworring-Bunk, Finite element modeling of the residual stress evolution in forged and direct-aged alloy 718 turbine disks during manufacturing and its experimental validation, in: AIP Conf. Proc., 2017: p. 070001. https://doi.org/10.1063/1.5008076.

[32] T. Depover, K. Verbeken, The effect of TiC on the hydrogen induced ductility loss and trapping behavior of Fe-C-Ti alloys, Corros. Sci. 112 (2016) 308–326. https://doi.org/10.1016/j.corsci.2016.07.013.

[33] E. Wallaert, T. Depover, M. Arafin, K. Verbeken, Thermal Desorption Spectroscopy Evaluation of the Hydrogen-Trapping Capacity of NbC and NbN Precipitates, Metall. Mater. Trans. A. 45 (2014) 2412–2420. https://doi.org/10.1007/s11661-013-2181-1.

[34] H.K.D.H. Bhadeshia, Prevention of Hydrogen Embrittlement in Steels, ISIJ Int. 56 (2016) 24–36. https://doi.org/10.2355/isijinternational.ISIJINT-2015-430.

[35] T. Depover, T. Hajilou, D. Wan, D. Wang, A. Barnoush, K. Verbeken, Assessment of the potential of hydrogen plasma charging as compared to conventional electrochemical hydrogen charging on dual phase steel, Mater. Sci. Eng. A. 754 (2019) 613–621. https://doi.org/10.1016/j.msea.2019.03.097.

[36] A. Drexler, S. He, V. Razumovskiy, L. Romaner, W. Ecker, R. Pippan, Verification of the generalised chemical potential for stress-driven hydrogen diffusion in nickel, Philos. Mag. Lett. 100 (2020) 513–523. https://doi.org/10.1080/09500839.2020.1808253.

[37] Y. Tateyama, T. Ohno, Atomic-scale effects of hydrogen in iron toward hydrogen embrittlement: Ab-initio study, ISIJ Int. 43 (2003) 573–578. https://doi.org/10.2355/isijinternational.43.573.

[38] J. Svoboda, G. Mori, A. Prethaler, F.D. Fischer, Determination of trapping parameters and the chemical diffusion coefficient from hydrogen permeation experiments, Corros. Sci. 82 (2014) 93–100. https://doi.org/10.1016/j.corsci.2014.01.002.

[39] D. Rudomilova, T. Prošek, P. Salvetr, A. Knaislová, P. Novák, R. Kodým, G. Schimo-Aichhorn, A. Muhr, H. Duchaczek, G. Luckeneder, The effect of microstructure on hydrogen permeability of high strength steels, Mater. Corros. 71 (2020) 909–917. https://doi.org/10.1002/maco.201911357.

[40] E. Van den Eeckhout, I. De Baere, T. Depover, K. Verbeken, The effect of a constant tensile load on the hydrogen diffusivity in dual phase steel by electrochemical permeation experiments, Mater. Sci. Eng. A. 773 (2020) 138872. https://doi.org/10.1016/j.msea. 2019.138872.

[41] Q. Liu, Q. Zhou, J. Venezuela, M. Zhang, A. Atrens, Hydrogen influence on some advanced high-strength steels, Corros. Sci. 125 (2017) 114–138. https://doi.org/10.1016/j.corsci. 2017.06.012.

[42] J.Y. Lee, W.Y. Choo, Thermal analysis of trapped hydrogen in pure iron, Metall. Trans. A. 13A (1982) 135–140.

[43] M. Nagumo, Hydrogen related failure of steels - A new aspect, Mater. Sci. Technol. 20 (2004) 940–950. https://doi.org/10.1179/026708304225019687.

[44] K. Takai, H. Shoda, H. Suzuki, M. Nagumo, Lattice defects dominating hydrogen-related failure of metals, Acta Mater. 56 (2008) 5158–5167. https://doi.org/10.1016/j.actamat. 2008.06.031.